Structure, electronic, and vibrational properties of amorphous AsS_2 and $AgAsS_2$: Experimentally constrained density functional study

J. Akola,[1,2,3,*] P. Jóvári,[4] I. Kaban,[5,6] I. Voleská,[7] J. Kolář,[7] T. Wágner,[7] and R. O. Jones[2,8]
[1]*Department of Physics, Tampere University of Technology, P.O. Box 692, FI-33101 Tampere, Finland*
[2]*Peter Grünberg Institut PGI-1 and JARA/HPC, Forschungszentrum Jülich, D-52425 Jülich, Germany*
[3]*COMP Centre of Excellence, Department of Applied Physics, Aalto University, FI-00076 Aalto, Finland*
[4]*Research Institute for Solid State Physics and Optics, P.O. Box 49, H-1525 Budapest, Hungary*
[5]*Institute of Materials Science, TU Dresden, D-01062 Dresden, Germany*
[6]*Institute for Complex Materials, IFW Dresden, P.O. Box 270116, D-01171 Dresden, Germany*
[7]*Department of General and Inorganic Chemistry, Faculty of Chemical Technology, University of Pardubice, Náměsti Československých legii 565, CZ-53210 Pardubice, Czech Republic*
[8]*German Research School for Simulation Sciences, FZ Jülich, D-52425 Jülich, Germany*
(Received 9 December 2013; revised manuscript received 4 February 2014; published 24 February 2014)

Density functional/molecular dynamics simulations and experimental data (x-ray and neutron diffraction, extended x-ray absorption fine structure) have been combined to determine structural and other properties of amorphous AsS_2 and $AgAsS_2$. These semiconductors represent the two small regions of the Ag-As-S ternary diagram where homogeneous glasses form, and they have quite different properties, including ionic conductivities. We find excellent agreement between the experimental results and large-scale (over 500 atoms) simulations, and we compare and contrast the structures of AsS_2 and $AgAsS_2$. The calculated electronic structures, vibrational densities of states, ionic mobilities, and cavity distributions of the amorphous materials are discussed and compared with data on crystalline phases where available. The high mobility of Ag in solid state electrolyte applications is coupled to the large cavity volume in AsS_2 and local modifications of the covalent As-S network in the presence of Ag.

DOI: 10.1103/PhysRevB.89.064202 PACS number(s): 61.43.Dq, 63.50.Lm, 71.15.Pd

I. INTRODUCTION

The electronic properties and applications of amorphous chalcogenides have been studied intensively for decades, and interest in the Ag-As-S system and its phase diagram goes back more than a century [1]. Solid state reactions of AgCl and As_2S_3 were used even earlier to prepare several compounds, including $AgAsS_2$ [2]. There has been particular focus recently on the changes in electronic properties with changing composition [3] and the relative importance of electronic and ionic conductivities. The dc conductivity of As-S glasses, for example, changes by several orders of magnitude on the addition of very small amounts of Ag [4], and the addition of Cu and Ag to chalcogenide glasses has led to materials in which ionic transport and redox reactions provide the basis for reconfigurable electronic devices and computer memory [5,6]. Mobile cations are created by anodic dissolution of the metal (e.g., $Ag \rightarrow Ag^+$), transported across the amorphous electrolyte layer, and reduced at the other electrode. Materials for these electrochemical metallization memories (ECM) or conductive bridge random access memories (CBRAM) include amorphous chalcogenides and oxides, and Cu and Ag are the most common metal ions [3,5,6].

Chalcogenide glasses along the $Ag_x(As_{0.33}S_{0.67})_{100-x}$ line have potential for ECM memory applications [7] and can be prepared as thin films by an optically induced solid state reaction [3]. Increasing the Ag concentration leads to dramatically increased conductivity in the range $9 < x < 15$, with Ag^+ ions playing a dominant role [8]. A combination of x-ray diffraction (XRD), neutron diffraction (ND), and x-ray absorption fine structure (EXAFS) has been used to study structural changes [9], and Raman [8,10] and scanning electron microscopy [10] measurements have been performed.

The Ag-As-S ternary phase diagram shows only two regions where homogeneous glass formation occurs: near $x = 0$ (AsS_2) and near $x = 25$ ($AgAsS_2$), the stoichiometric composition $(As_2S_3)_{0.5}(Ag_2S)_{0.5}$ [11]. Glasses with $4 < x < 20$ segregate on a micrometer scale [10]. Crystalline forms of the silver sulfarsenide $AgAsS_2$ occur in nature as smithite (monoclinic) [12] and trechmannite (rhombohedral) [13], and refinement of the original structures [12,13] has resulted in significantly better R factors [14]. Glasses along the Ag_2S-As_2S_3 tie line, including $AgAsS_2$, have been studied by differential calorimetry and XRD [15], modulated differential scanning calorimetry and Raman spectroscopy [8], EXAFS [16], ND [17,18], and XRD [19]. Optical and photoemission studies [20] have been carried out on amorphous (a-) and crystalline (c-) $AgAsS_2$.

Understanding the properties of *any* glass, not only Ag-As-S, requires a detailed knowledge of its structure. This is provided here for AsS_2 and $AgAsS_2$ by combining experimental measurements (EXAFS, XRD, and ND) with extensive density functional (DF)/molecular dynamics (MD) simulations of samples with more than 500 atoms. This experimentally constrained DF approach treats the geometrical and electronic structures on equal footings and has been applied successfully in $Ge_2Sb_2Te_5$ [21], $Ag_{3.5}In_{3.8}Sb_{75.0}Te_{17.7}$ [22], and $Ga_{11}Ge_{11}Te_{78}$ alloys [23]. Electronic structure constraints proved to be crucial in semiconducting $Ge_2Sb_2Te_5$ [21], since reverse Monte Carlo analysis alone led to excellent agreement with XRD data, but an unphysical metallic band structure. The

*jaakko.akola@tut.fi

simulation trajectories allow us to calculate the vibrational densities of states and the self-diffusion coefficients, as well as the electronic and geometrical structures, including the distribution of cavities (voids) that provide "free" volume for atomic diffusion. Drabold and co-workers [24,25] have simulated the mobility of Ag^+ (and Cu^+) cations in Ge/Se liquids and glasses at several temperatures and have found that the most diffusive ions prefer low density regions of the networks ("trapping centers"). The ordering of oxygen vacancies may also play an essential role in the formation of conductive filaments in a TiO_2 resistive switching memory cell [26]. The present calculation is the first in an ongoing study of Ag^+ mobility and conductivity in chalcogenide glasses.

II. METHODS

A. Experiment

Samples of amorphous AsS_2 and $AgAsS_2$ were prepared from appropriate amounts of the high purity (99.999%) constituent elements and placed in silica ampoules that were then evacuated (residual pressure $\sim 10^{-4}$ Pa) and sealed. Oxide formation in As was avoided by sublimation of the sample before weighing. The samples were melted in a rocking furnace, held at 1223 K for 24 h, and quenched in air. The glassy samples were then annealed for 3 h near the glass transition temperature and kept under an inert atmosphere of N_2 after breaking the ampoules. The mass density was determined with an accuracy of 0.15% using the Archimedean method by weighing samples in air and in toluene.

X-ray diffraction (XRD) measurements of flat samples ($\sim$2 mm thick) were carried out in transmission geometry at the BW5 beamline at HASYLAB (DESY, Hamburg, Germany). The incident beam had an energy of 100 keV and a cross section of 2 mm^2. The scattered intensity was recorded by a Ge solid-state detector, and the raw data were corrected for background, absorption, polarization, detector dead time, and variations in detector solid angle [27]. The neutron diffraction (ND) experiments were performed with the 7C2 diffractometer at the Laboratoire Léon Brillouin (CEA-Saclay, France). The samples were ground and filled into thin-walled (0.1 mm) vanadium containers of 7 mm diameter. The diffraction data were corrected for detector efficiency, empty instrument background, scattering from the sample holder, multiple scattering [28], and absorption [29] using standard procedures [30].

The As and Ag K-absorption edge EXAFS measurements were carried out at the X1 experimental station at HASYLAB in transmission mode. The glassy alloys were finely ground, mixed with cellulose, and pressed into tablets. The quantity of powder was selected to provide transmission near $1/e$ for the particular composition and absorption edge. EXAFS spectra were obtained in steps of 0.03 Å^{-1} above the absorption edge, and the measuring time was k weighted during data collection. The x-ray absorption cross sections $\mu(E)$ were converted to $\chi(k)$ by standard procedures using the program Viper [31].

B. Density functional calculations

The DF/MD simulations (constant particle number N, constant volume V) used the CPMD program package [32] with Born-Oppenheimer molecular dynamics (time step 3.025 fs, 125 a.u.) and the PBEsol approximation [33] for the exchange-correlation energy. The electron-ion interaction was described by scalar-relativistic pseudopotentials of Troullier-Martins form [34] with valence configurations Ag: $4d^{10}5s$, As: $4s^24p^3$, and S: $3s^23p^4$. We use periodic boundary conditions with a single point ($\mathbf{k} = 0$) in the Brillouin zone, and the kinetic energy cutoffs of the plane wave basis set were 60 Ry in $AgAsS_2$ and 25 Ry in AsS_2. The temperature is controlled by a Nosé-Hoover thermostat (frequency 800 cm^{-1}, chain length 4) [35].

The $AgAsS_2$ system comprised 560 atoms (140 Ag, 140 As, 280 S) and 3920 valence electrons. The size of the cubic box (23.122 Å) corresponds to a density of 0.0453 atoms/Å^3 (4.644 g/cm^3). The AsS_2 system has 540 atoms (180 As, 360 S, 3060 valence electrons) in a cubic box of size 24.0747 Å^3 (0.0388 atoms/Å^3, 2.968 g/cm^3). The simulations began at temperatures below the melting points, and the starting structures were generated by applying the reverse Monte Carlo method to the experimental data set (see below). The $AgAsS_2$ sample was heated to 500 K and cooled to 300 K over 125 ps in steps of 50 K. Data were collected at 300 K for 37.8 ps (12 500 time steps), and the structure was then optimized. The AsS_2 sample was cooled from 600 K in steps of 50 K. The cooling time to 300 K was 100 ps, and final data were collected over 30.3 ps (10 000 time steps).

The power spectra (vibrational densities of states) and their projections onto the elements were calculated from the Fourier transform of the velocity-velocity autocorrelation functions from the final trajectories. The self-diffusion coefficients were determined from the time dependence of the atomic mean square displacements. Cavities are assigned by determining domains that are farther from any atom than a given cutoff (here 2.5 Å) and building cells around their centers according to the Voronoi construction [36].

C. RMC refinement

The starting structures for DF/MD simulations were produced by applying reverse Monte Carlo (RMC) simulation [37,38], in which the atoms are moved randomly to optimize the fit to high energy XRD and As K-edge EXAFS data in AsS_2. For $AgAsS_2$ we also used ND and Ag K-edge EXAFS data [9]. Several structures were optimized by the DF method in order to select promising starting points for MD annealing. The time scale of traditional melt-quench simulations is much too short for physical processes that can take hours in these materials, and we start from an atomic model based on some prior knowledge. We use MD to shake the system and allow local diffusion and relaxation *without* melting.

After the DF/MD simulations, the structure determined from the DF minimum energy was refined by RMC, where electronic structure and other information can be incorporated by constraining coordination numbers or bond angle distributions, and the bond angles here were constrained to be close to those of the unmodified DF structure. The minimum distances were As-As: 2.20 Å, As-S: 2.0 Å, and S-S: 1.85 Å, and the maximum displacement of an atom in a move was 0.01 Å along each coordinate. Refinement was stopped after $\sim$25 000 accepted moves. The total energy of the final RMC fit was 37 meV/atom higher than the DF energy minimum in $AgAsS_2$, and 22 meV/atom higher in AsS_2. These energy differences are within the range of thermal fluctuations at 300 K ($\sim k_B T$), and the RMC refined structures are very close to the DF structures with minimum energy. The use of DF optimized structures as RMC input is particularly advantageous in these systems, where the scattering of x rays and neutrons is much weaker in one element (S) than in the others.

III. RESULTS

A. Neutron and x-ray diffraction, EXAFS

The structure factors $S(Q)$ for a-AsS_2 (XRD) and a-$AgAsS_2$ (XRD, ND) (Fig. 1) show halo patterns typical of disordered materials, and the oscillations extend well beyond 10 Å^{-1}. The prepeak at 1.0 Å^{-1} in the AsS_2 XRD structure is typical for glassy materials and reflects the intermediate range ordering of coordination polyhedra, as seen in amorphous silica for a network of corner-sharing tetrahedra. The prepeak appears as a shoulder in the ND structure factor of $AgAsS_2$ and as a threshold in XRD and is reproduced by the calculations. The overall agreement between the measured and calculated curves is very good. The corresponding pair distribution functions (PDF) determined by Fourier transformation are presented as Supplementary Information (Fig. SF1) [39].

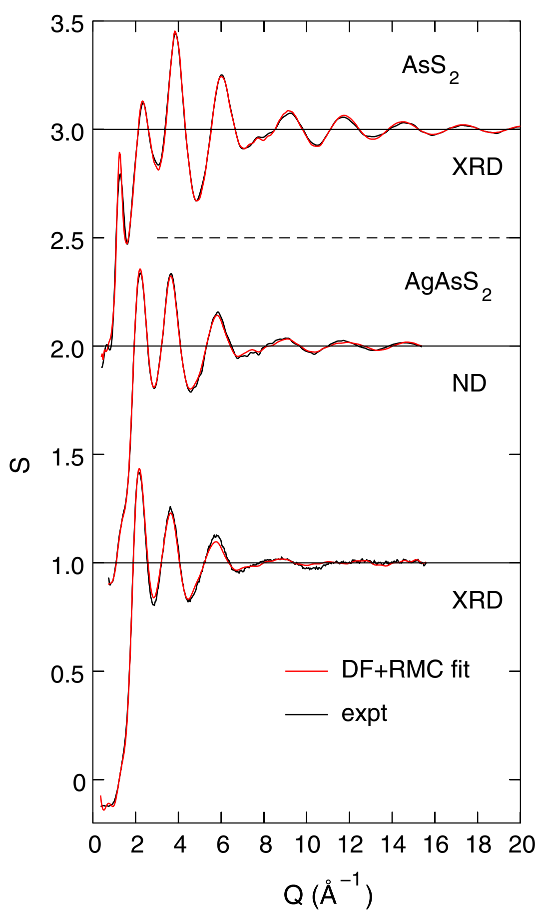

FIG. 1. (Color online) Structure factors $S(Q)$ for a-AsS_2 (XRD) and a-$AgAsS_2$ (XRD, ND). Black line: Experiment, red line: calculated (DF+RMC fit). The upper two curves are displaced by 1 and 2 units, respectively.

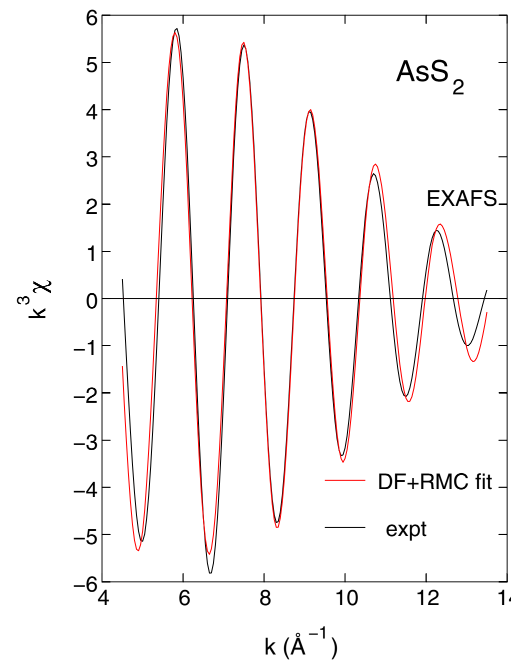

FIG. 2. (Color online) Experimental As K-edge EXAFS spectra of a-AsS_2 (black) compared with DF-RMC refined model (red).

Excellent agreement is also found for the amplitude and phase of the As and Ag K-edge EXAFS spectra of a-AsS_2 (Fig. 2) and a-$AgAsS_2$ (Fig. 3), indicating that the local configurations around Ag and As (and the corresponding bond distances) are described well. These results show that all aspects of the experimental data set are satisfied by our atomic models.

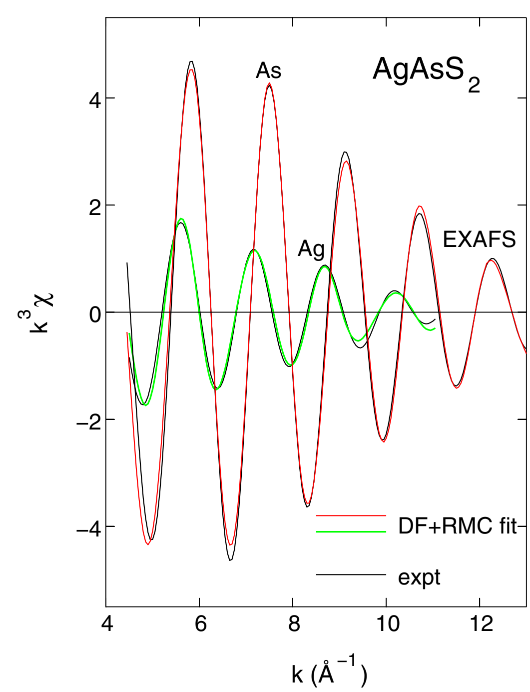

FIG. 3. (Color online) DF-RMC refined model Ag (green, thick line) and As (red line) K-edge EXAFS spectra of a-$AgAsS_2$ compared with experiment (black lines).

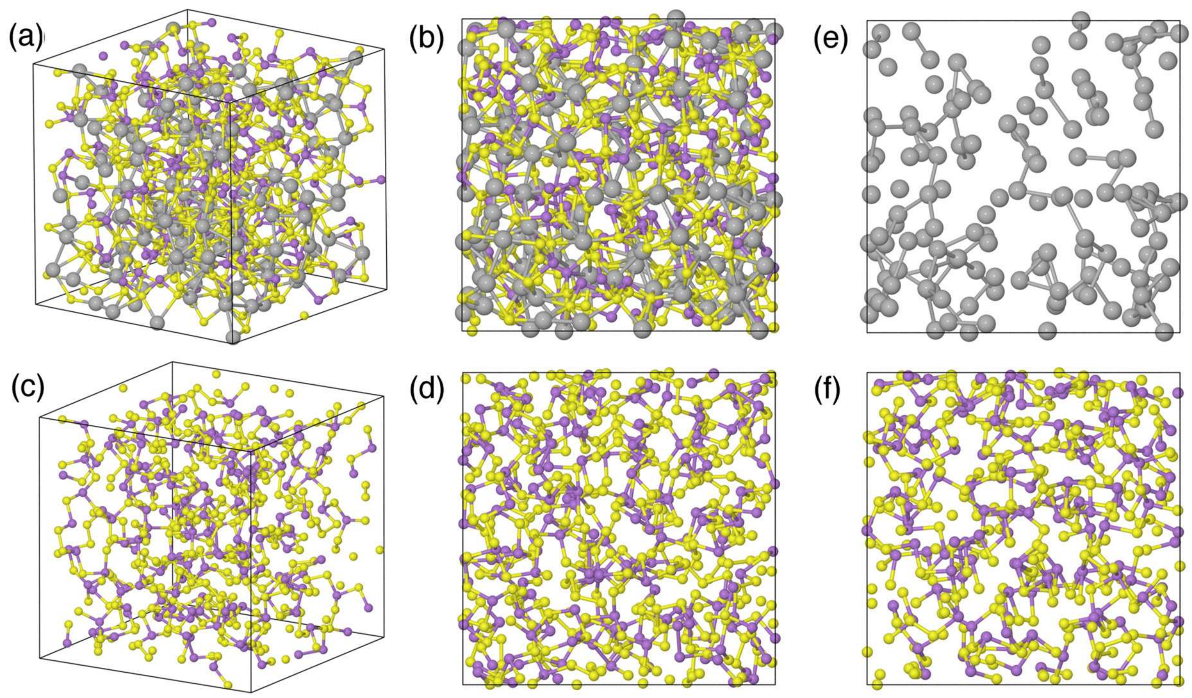

FIG. 4. (Color online) Structures of (a) and (b) a-$AgAsS_2$ and (c) and (d) a-AsS_2. The simulation boxes comprise 560 (side 23.1 Å) and 540 atoms (24.1 Å), respectively. (e) Ag atoms and (f) As and S atoms in a-$AgAsS_2$. Ag: gray, As: magenta, S: yellow.

B. Structure: Pair distribution functions, coordination numbers

Two views of the final structures of AsS_2 and $AgAsS_2$ are shown in Figs. 4(a)–4(d). Also shown for $AgAsS_2$ are the Ag atoms alone and the As-S network [Figs. 4(e) and 4(f)]. Ag forms stringlike metallic units, and over 90% of the Ag atoms have an Ag neighbor. The connectivity in the As-S network in $AgAsS_2$ differs from that in AsS_2 in having terminal sulfur atoms. $AgAsS_2$ has a higher density and is more densely packed than AsS_2. The partial PDF $g_{\alpha\beta}(r)$ for As-S, As-As, S-S in AsS_2 and $AgAsS_2$ are shown in Fig. 5 and for Ag atoms in $AgAsS_2$ (Ag-Ag, Ag-S, Ag-As) in Fig. 6. The first maximum and the first minimum (bond cutoff) of each curve are given in Table I. The Ag-As PDF has a weak shoulder, and the first maximum and minimum could not be assigned.

The local coordination shows many interesting details. In a-AsS_2, the As atoms are predominantly (98.8%) threefold coordinated, mainly as As-S_3 (81.8 %) and As-AsS_2 configurations (16.4 %), while S atoms are almost all twofold coordinated (39.9% S-AsS, 49.8% S-As_2). The average coordination numbers in AsS_2 and $AgAsS_2$ are given in Table II. The situation is more complicated in ternary $AgAsS_2$, where the dominant configurations are given in Table III. Ag atoms favor coordination numbers between 5 and 7 (mainly Ag-Ag_2S_4, Ag-AgS_4, Ag-AgS_5, and Ag-Ag_2S_5), which are significantly

TABLE I. The first maxima of the partial PDF $g_{\alpha\beta}$ of a-$AgAsS_2$ and a-AsS_2 at 300 K. Bond cutoffs: As-As: 2.8, As-S: 2.7, As-Ag: 3.0, As-S: 2.3, Ag-S; 3.3, Ag-Ag: 3.6. All distances in Å.

	α	$\beta =$ As	S	Ag
$AgAsS_2$	As	2.53	2.28	–
	S	2.28	2.06	2.55
	Ag	–	2.55	3.02
AsS_2	As	2.53	2.29	–
	S	2.29	2.07	–

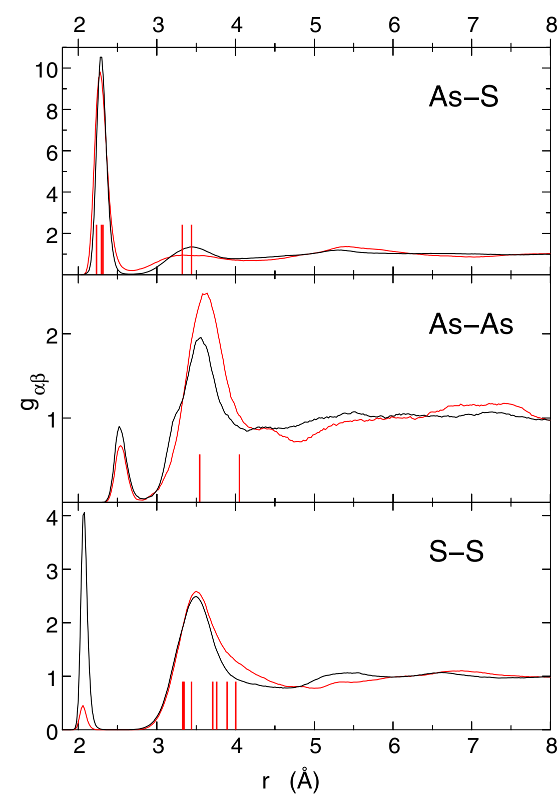

FIG. 5. (Color online) Partial PDF $g_{\alpha\beta}(r)$ in a-AsS_2 (black line) and a-$AgAsS_2$ (red line). Vertical red bars show interatomic separations in trechmannite (c-$AgAsS_2$, Ref. [14]).

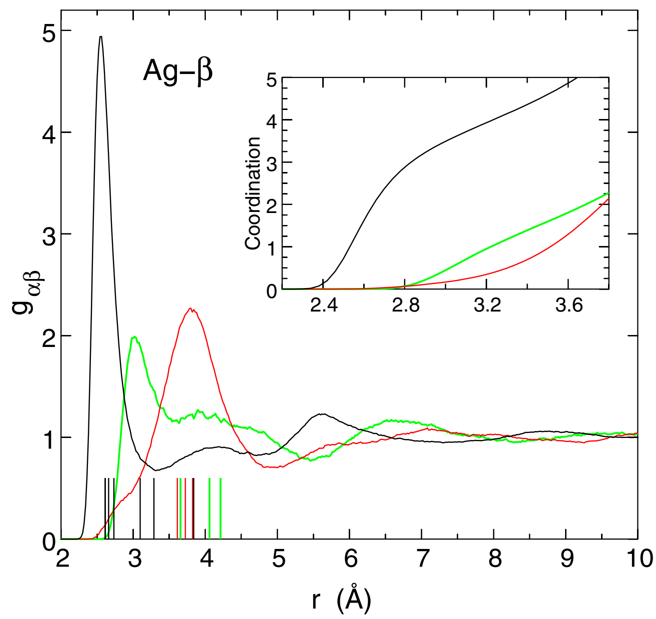

FIG. 6. (Color online) Partial PDF $g_{\alpha\beta}(r)$ for Ag-α distances in a-$AgAsS_2$: Black line: Ag-S, red line: Ag-As, green line (thick): Ag-Ag. Inset: Coordination number as function of bond cutoff distance. Interatomic separations in trechmannite (c-$AgAsS_2$, Ref. [14]) are shown in the corresponding colors.

higher than the fourfold coordination found in earlier ND measurements [17]. As atoms are mainly threefold to fourfold coordinated (with As-S_3 as the most prominent configuration). The most prevalent environments of S atoms involve threefold to fivefold coordination: S-Ag_3As, S-Ag_2As_2, and S-$AgAs_2$ have almost equal weights, S-Ag_4As and S-Ag_2As are less prominent.

The local atomic order in a-$AgAsS_2$ can be compared with that in the crystalline forms smithite (24 $AgAsS_2$ units in the unit cell) and trechmannite (12 units), which have numerous nonequivalent bond lengths. The density of a-$AgAsS_2$ (4.644 g/cm^3) is closer to the density of trechmannite (4.726 g/cm^3) [14] than that of smithite (5.073 g/cm^3) [14], and we use trechmannite for comparison purposes. The Ag atom in trechmannite has four S nearest neighbors [2.628 Å (3), 2.732 Å] with distorted tetrahedral symmetry (Ag-S_4 average 2.654 Å), and two more distant S neighbors [3.097 Å, 3.288 Å]. Three such tetrahedra are linked by common S atoms. As and its three nearest S neighbors form a trigonal AsS_3 pyramid (mean distance 2.281 Å) with additional S atoms at 3.322, 3.439 Å. By sharing S atoms, three such pyramids form an As_3S_6 ring with $\sim C_{3v}$ symmetry, higher than the symmetry of these rings in smithite ($\sim C_s$). The As-S bond lengths inside the ring average 2.305 Å, and the external bonds are 2.233 Å. The structure of trechmannite can then be viewed as layers of As_3S_6 rings linked by AgS_4 tetrahedra. Other bond lengths of interest are: Ag-Ag: 3.656, 4.060, 4.212 Å; As-As: 3.543, 4.048 Å; Ag-As: 3.612, 3.723, 3.825, 3.838 Å; S-S: 3.329, 3.344, 3.440, 3.709, 3.760 Å [14]. All these interatomic separations are shown in Figs. 5 and 6.

Figures 5 and 6 and Table I show that short homonuclear bonds that occur in amorphous $AgAsS_2$ are absent in the crystal. The weak S-S minimum at 2.06 Å is close to the S-S bond length in amorphous sulfur (2.05–2.06 Å) [40,41] and in small sulfur chains and rings [42]. The second peak in the As-As and Ag-Ag PDF are in the same range as these atom separations in the crystal, and the As-S distance (2.28 Å) is close to As-S bonds measured in trechmannite [14] as well as in Ge-As-S glasses and the corresponding crystals [43,44].

The sulfur coordination (Table II) is significantly higher in $AgAsS_2$ (~3.6) than in AsS_2 (twofold), due to Ag-S bonds and a different As-S network. AsS_2 has a significant fraction of S-S bonds, which are almost absent in $AgAsS_2$. These bonds are not compensated by covalent As-S bonds and lead to terminal S atoms (48% of all S atoms) in the As-S network [Fig. 4(f)]. The contribution of As-As bonds is small in both alloys, and the effect of Ag content on As coordination is quite subtle. The missing first peak in the As-Ag PDF indicates that bonds between As and Ag are not favored.

TABLE II. The average coordination number $N_{\alpha\beta}$ in a-$AgAsS_2$ and a-AsS_2 at 300 K. Cutoff distances as in Table I.

	α	$N_{\alpha \mathrm{As}}$	$N_{\alpha \mathrm{S}}$	$N_{\alpha \mathrm{Ag}}$	$N_{\alpha,\mathrm{tot}}$
$AgAsS_2$	As	0.12	2.95	0.17	3.23
	S	1.48	0.06	2.07	3.60
	Ag	0.17	4.14	1.81	6.11
AsS_2	As	0.18	2.85	–	3.03
	S	1.42	0.59	–	2.01

C. Angular distributions

The angular distributions of Ag-S and As-S bonds at 300 K are shown in Fig. 7 (DF/MD simulations). The broad distributions for Ag reflect metallic binding [Fig. 7(a)], and there is a maximum at 60° for Ag-Ag-Ag configurations corresponding to triangular clusters. The S-Ag-S distribution peaks at a relatively small angle (70°), whereas the Ag-S-Ag distribution has a maximum at 90° and less weight at smaller values.

The bond angles in the As-S network [Fig. 7(b)] differ little in AsS_2 and $AgAsS_2$. The angles around sulfur peak below 100°, whereas the S-As-S angles have maxima above 100° and more weight at larger values up to 135°. Both distributions indicate pyramidal configurations, and we note that stoichiometric c-As_2S_3 has bond angles near 99° for both elements. The coordination of As and S is less than four, which means that there is no contribution from tetrahedral configurations (109.47°). For AsS_2, there is a small peak at 90° in S-As-S corresponding to configurations with nearly octahedral (cubic) bond angles. Despite the numerous S-S bonds there are few signs of triangular configurations (60°) in the As-S network.

D. Cavity distributions

The presence of cavities (vacancies, voids) and their distribution have significant effects on the properties of materials and have not yet been discussed in AsS_2 and $AgAsS_2$. We show the corresponding distributions in Fig. 8, calculated using a cutoff of 2.5 Å and the Voronoi construction [36]. AsS_2 has a

TABLE III. Percentage of atoms of element α with coordination number N_α, and dominant configurations in a-$AgAsS_2$ at 300 K (DF/MD simulations, values under 1% are excluded). Bond cutoffs as in Table I. Boldface: total coordination number.

α	$N_\alpha = 2$	3	4	5	6	7	8	9
As		**81.2**	**17.8**					
		S_3: 73.4	AgS_3: 11.9					
		AsS_2: 7.7	S_4: 3.1					
			$AgAsS_2$: 2.1					
S	**6.0**	**28.3**	**40.8**	**19.5**	**4.6**			
	As_2: 4.1	$AgAs_2$: 18.7	Ag_3As: 19.6	Ag_4As: 12.1	Ag_5As: 2.4			
		Ag_2As: 8.7	Ag_2As_2: 18.9	Ag_3As_2: 5.4	Ag_3AsS: 1.0			
Ag		**1.0**	**9.7**	**24.6**	**32.3**	**21.0**	**8.0**	**2.7**
			S_4: 5.3	AgS_4: 12.8	Ag_2S_4: 13.0	Ag_2S_5: 7.6	Ag_4S_4: 2.7	Ag_5S_4: 1.1
			AgS_3: 2.8	Ag_2S_3: 4.7	AgS_5: 9.6	Ag_3S_4: 6.7	Ag_3S_5: 2.4	
				S_5: 3.3	Ag_3S_3: 3.7	Ag_4S_3: 2.0		

much lower density and a much larger cavity volume (37.8 %) than $AgAsS_2$ (4.8%) and is clearly porous at the atomistic level. The cavity volume of a-SiO_2 was 31.9% with the same parameter set [45].

The trechmannite structure may be viewed as a defective PbS (galena) structure. The defects are vacancies: one on an Ag site surrounded by six S atoms, the second an S site surrounded by six As atoms. To test whether this effect occurs in the amorphous state, we have calculated partial PDF involving cavity centers, and they are shown in the Supplementary Information (Fig. SF4) [39], together with the corresponding coordination numbers (Table S1). All atom types have comparable PDF weights near the cavities, but the cavity-S coordination number is highest (2.4). The overall

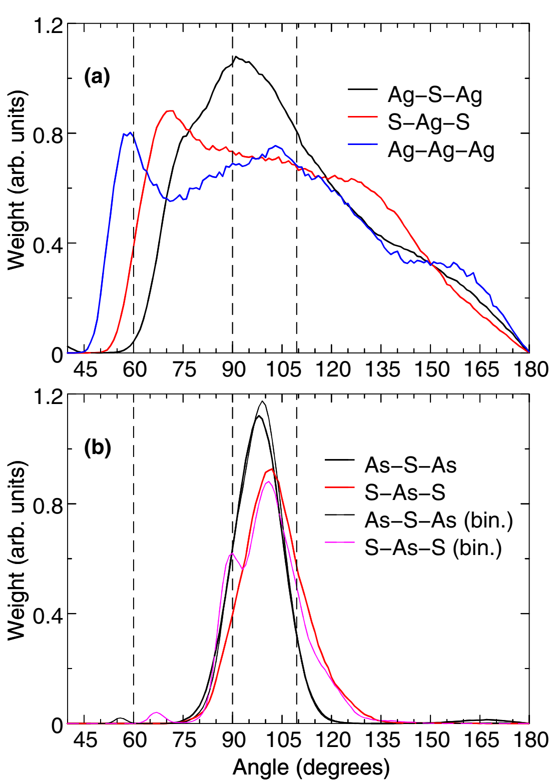

FIG. 7. (Color online) Angular distributions in AsS_2 (bin.) and $AgAsS_2$. The dashed lines denote the values 60°, 90°, and 109.47° (tetrahedral).

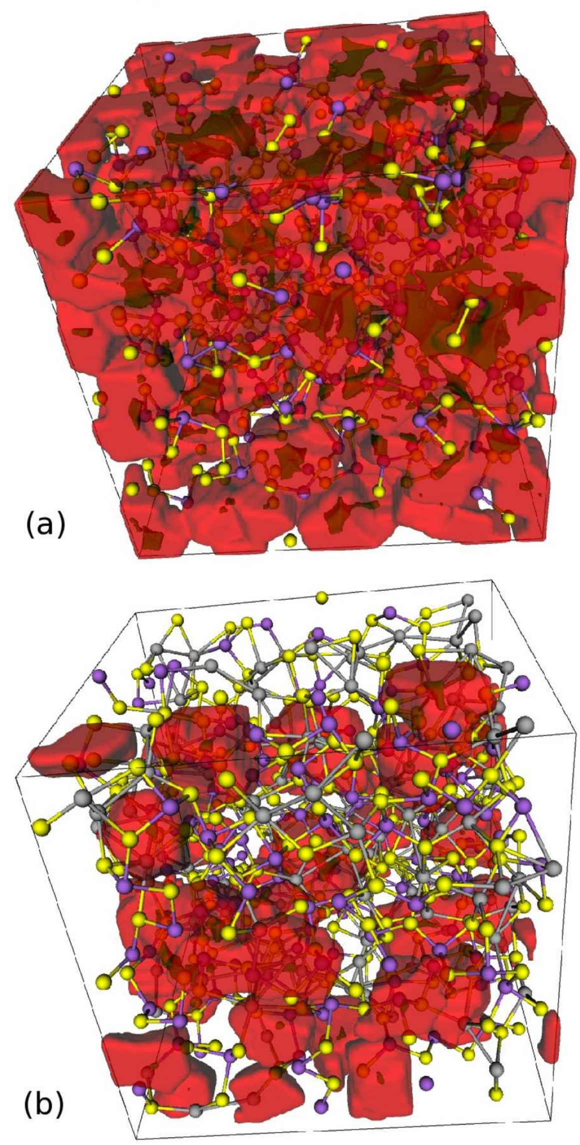

FIG. 8. (Color online) Cavities (red) in DF-RMC optimized structures of (a) a-AsS_2, (b) a-$AgAsS_2$. Yellow: S, purple: As, silver: Ag.

cavity coordination is close to sixfold as in trechmannite, but the nearest neighbors are mixed in a-AgAsS_2. In spite of the relatively high Ag concentration, many Ag cations (∼40%) are adjacent to cavities, which would increase their mobility in the As/S matrix. The small cavity-cavity coordination number (<0.2) demonstrates the absence of multicavities, as opposed to the situation in AsS_2.

E. Dynamical properties

The high mobility of Ag in semiconducting materials is of particular technological interest, and analysis of the present MD trajectories gave the following values of the self-diffusion coefficient of Ag: 3.71 (at 600 K), 2.87 (500 K), 2.02 (450 K), and 1.31 (400 K), in units of 10^{-6} cm^2/s. These values are an order of magnitude higher than those in As and S. At 600 K, for example, we find 0.31 (As) and 0.45 (S), in the same units. As and S atoms are almost immobile at lower temperatures, while Ag atoms continue to diffuse.

The Raman and infrared active vibrational modes in crystalline AgAsS_2 have been studied by Slivka *et al.* [46]. There are numerous modes of each type in the range 20–400 cm^{-1}, and there are distinctive lines between 260 and 400 cm^{-1} that are strong in Raman and fairly clear in the IR spectra. The frequencies of Raman active modes have been measured in a-AsS_2 and a-AgAsS_2 [8,10,47]. Adding Ag to AsS_2 leads to a new feature (∼375 cm^{-1}) above the main feature in AsS_2 (350^{-1}). Infrared absorption and reflection spectra show transverse optical modes at 164 and 310 cm^{-1} [48].

The calculated power spectra (vibrational densities of states, vDOS) and their projections onto the elements at 300 K are shown for a-AsS_2 and a-AgAsS_2 in Fig. 9. We emphasize that the vDOS includes all frequencies with equal weights and does not reflect the actual intensities of Raman and IR active modes. The qualitative features in AsS_2 can readily be identified: S-S vibrations with frequencies near 450 cm^{-1}, a broad distribution with a peak near 320 cm^{-1} (As-S vibrations), and a broad low energy peak involving modes with several atoms. The frequency range of the S-S vibrations covers the frequencies found in sulfur chains [42]. Apart from the low-frequency modes involving Ag, the power spectrum for AgAsS_2 (Fig. 9) shows a remarkably broad and uniform spectrum. The presence of Ag changes the vibrational properties of sulfur significantly; there are numerous Ag-S bonds and very few S-S bonds. The skewed maximum in the Ag projection at low frequencies (∼50 cm^{-1}) indicates a flat potential energy surface and weak restoring forces, so that Ag atoms should be mobile if the temperature is increased and/or an external electric field applied.

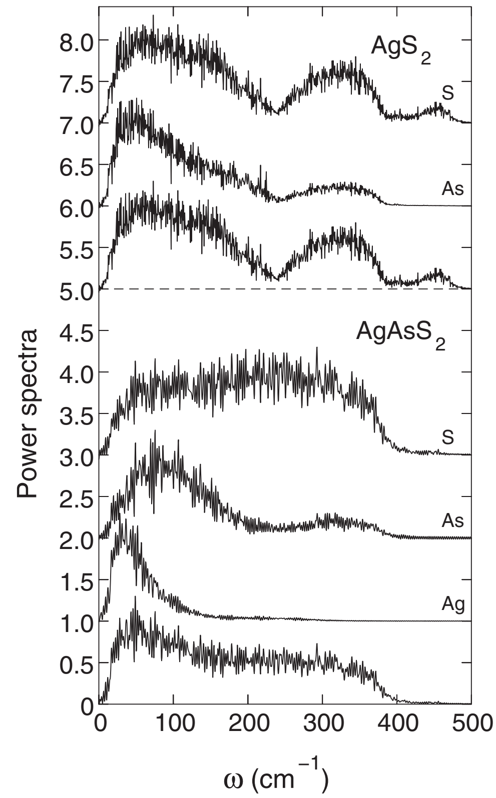

FIG. 9. Computed vibrational density of states of amorphous AsS_2 and AgAsS_2 at 300 K with projections onto elements. All curves have the same maximum.

F. Electronic structure, density of states

The calculated electronic densities of states (DOS) of AsS_2 and AgAsS_2 are shown in Fig. 10, together with projections onto s-, p-, and d-atomic functions. The band gap in AsS_2 is 1.3 eV. There appear to be no crystalline forms of AsS_2, but the optical band gap in crystalline As_2S_3 (orpiment) is 2.6 eV [49]. The calculated band gap in a-AgAsS_2 (1.0 eV) can be compared with the measured band gaps in the amorphous (1.95 eV) and crystalline (smithite, 2.1 eV) phases [50]. Density functional calculations with the PBEsol approximation commonly lead to gaps in the spectrum of Kohn-Sham eigenvalues that are less than measured optical band gaps. The superposition of x-ray spectra (fluorescent K bands and L_{23} emission bands of S) on a common energy scale [19,51] provide information about the density of states in c-AgAsS_2 (smithite). There are prominent peaks at −13 eV (S) and −4.1 eV (Ag) that are also present in our results. Furthermore, the K-band spectra of amorphous and crystalline AgAsS_2 are very similar [19]. The origin of the peaks has been determined by electronic structure calculations [52] on clusters with the bulk crystalline (smithite) structure [51].

The differences in DOS between the two samples can readily be interpreted. The prominent peak at −4 eV arises from the 4d shell in Ag, while the more structured and narrower lower valence bands in AgAsS_2 are consistent with the reduced number of homopolar bonds (s-s overlap). This effect has been found previously in c- and a-$Ge_2Sb_2Te_5$ [36]. The effective charges in AgAsS_2, evaluated using the Bader approach [53], are Ag: $+0.37e$, As: $+0.12e$, and S: $-0.24e$. The S charges are distributed in two "bands" around $-0.10e$ and $-0.35e$, where the latter corresponds to terminal S atoms. The values for AsS_2, where there are no such atoms, are $+0.10e$ (As) and $-0.05e$ (S). The presence of the Ag cation causes a charge transfer to S as the covalent As-S network breaks up. The ionic character of Ag-S bonding is confirmed by the computed chemical bond orders (bond strengths), which lie in the range 0.2–0.5, while the covalent As-S bonds have values above unity (the value for

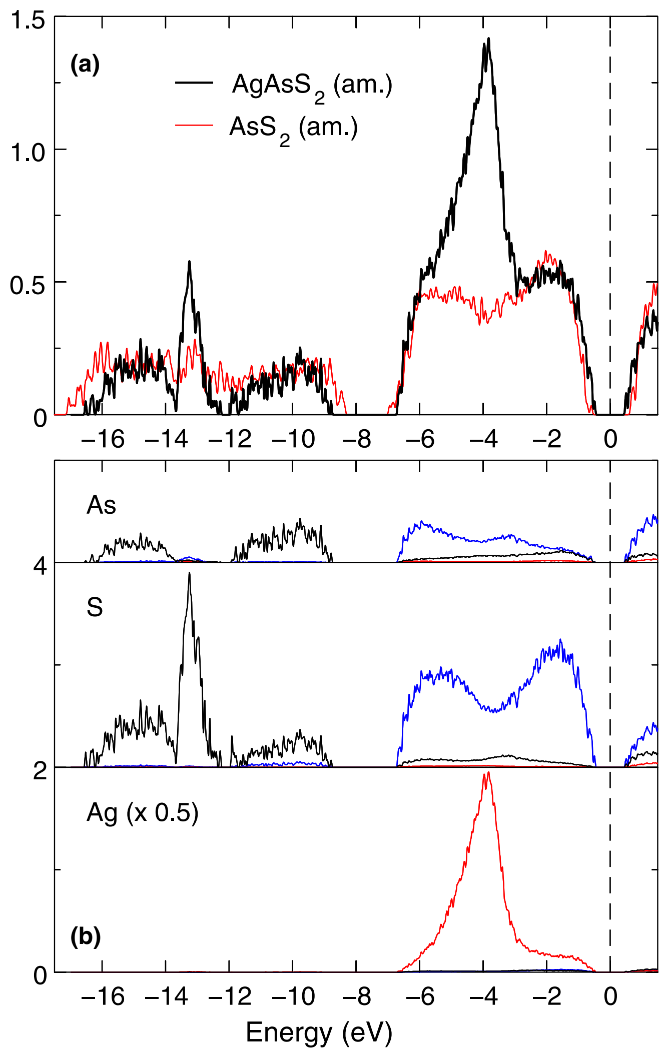

FIG. 10. (Color online) (a) Computed electronic densities of states of a-AsS_2 (red line) and a-$AgAsS_2$ (black line) with (b) projections onto elements and atomic orbitals for a-$AgAsS_2$. Black: s, blue: p, red: d.

a single covalent bond). The terminal S atoms in $AgAsS_2$ are evident with higher values (>1) in the As-S bond orders. Plots of bond orders are given in the Supplementary Information (Figs. SF2 and SF3) [39].

IV. DISCUSSION AND CONCLUDING REMARKS

The combination of MD/DF simulations and experimental measurements using RMC refinement incorporates the electronic structure into structure determination. It has been applied successfully to amorphous $Ge_2Sb_2Te_5$ [21], $Ag_{3.5}In_{3.8}Sb_{75.0}Te_{17.7}$ [22], and $Ga_{11}Ge_{11}Te_{78}$ alloys [23], and has been used here to study amorphous AsS_2 and $AgAsS_2$. The resulting models (540 atoms in AsS_2, 560 atoms in $AgAsS_2$) are unusually large for combined DF/MD simulations, in order to reduce the effects of periodic boundary conditions and enable local density fluctuations. The models satisfy all criteria for agreement between theory and experiment (structure factors, EXAFS signals, DF energy, band gap) extremely well, and the calculated power spectra are in reasonable agreement with optical absorption and Raman spectra. The calculated self-diffusion constants show that Ag ions are much more mobile than As and S ions.

The As-S network and the cavities are crucial aspects to understand the atomic structure of AsS_2 and $AgAsS_2$. AsS_2 shows ideal twofold coordination for S and threefold coordination for As, with numerous S-S bonds (0.6). The As-S network differs in $AgAsS_2$; there are almost no S-S bonds, terminal S atoms coordinate with Ag, and the average coordination of S (3.6) is much larger. Furthermore, the abundant cavities in AsS_2 (38%) are natural locations for Ag cations, and most are occupied by Ag in $AgAsS_2$. The calculated electronic DOS and the effective atomic charges support this picture.

The results suggest two main reasons for the high mobility of Ag^+ (and Cu^+) cations in solid state electrolytes: Cavities can act as trapping sites in the host material [24,25] and provide space for mobility, and cations can alter locally the bonding in the host. In the context of ECM/CBRAM materials, Ag^+ (Cu^+) can both move through the cavities in the host electrolyte and break covalent bonds in the material. We are extending the present calculations to quantify the role of Ag^+ in the electrical conductivity of Ag-doped semiconductors.

ACKNOWLEDGMENTS

We acknowledge gratefully the computer time provided by the JARA-HPC Vergabegremium on the JARA-HPC partition of the supercomputer JUQUEEN at Forschungszentrum Jülich, and for time granted on the supercomputer JUROPA at Jülich Supercomputer Centre. We thank H. Effenberger for providing Ref. [14]. We acknowledge financial support from the Academy of Finland through its Centres of Excellence Program (Project 251748) (J.A.), the Hungarian Basic Research Fund OTKA (Grant 083529) (P.J.), and Grant CZ.1.07/2.3.00/20/0254 realized by the European Science Foundation (ESF) and the Ministry of Education, Youth and Sports of the Czech Republic. The German Research School for Simulation Sciences is a joint venture of the FZ Jülich and RWTH Aachen University.

[1] F. M. Jaeger and H. S. van Klooster, Z. Anorg. Chem. **78**, 245 (1912).
[2] H. Sommerlad, Z. Anorg. Allg. Chem. **18**, 420 (1898).
[3] M. Frumar and T. Wágner, Curr. Opinion Solid State Mater. Sci. **7**, 117 (2003), and references therein.
[4] Y. Kawamoto, N. Nagura, and S. Tsuchihashi, J. Am. Ceram. Soc. **57**, 489 (1974), and references therein.
[5] R. Waser, R. Dittmann, G. Staikov, and K. Szot, Adv. Mater. **21**, 2632 (2009).
[6] W. Lu, D. S. Jeong, M. Kozicki, and R. Waser, MRS Bull. **37**, 124 (2012), and references therein.
[7] J. Kolář, J. M. Macák, K. Terabe, and T. Wágner, J. Mater. Chem. C **2**, 349 (2014).
[8] C. Holbrook, P. Chen, D. I. Novita, and P. Boolchand, IEEE Trans. Nanotech. **6**, 530 (2007), and references therein.

[9] I. Kaban, P. Jóvári, T. Wágner, M. Bartoš, M. Frumar, B. Beuneu, W. Hoyer, N. Mattern, and J. Eckert, J. Non-Cryst. Solids **357**, 3430 (2011), and references therein.
[10] F. Kyriazis, A. Chrissanthopoulos, V. Dracopoulos, M. Krbal, T. Wágner, M. Frumar, and S. N. Yannopoulos, J. Non-Cryst. Solids **355**, 2010 (2009).
[11] Y. Kawamoto, M. Agata, and S. Tsuchihashi, J. Ceram. Soc. Jpn. **82**, 502 (1974).
[12] E. Hellner and H. Burzlaff, Naturwiss **51**, 35 (1964).
[13] T. Matsumoto and W. Nowacki, Z. Kristallog. **129**, 163 (1969).
[14] H. Fric, Diplomarbeit, Universität Wien, Austria, 2002.
[15] I. S. Kovaleva, L. D. Popova, N. P. Luzhnaya, V. V. Sukhankina, and L. I. Antonova, Inorg. Mater. (USSR) **7**, 1340 (1971).
[16] V. Mastelaro, S. Bénazeth, and H. Dexpert, J. Non-Cryst. Solids **185**, 274 (1995).
[17] I. T. Penfold and P. S. Salmon, Phys. Rev. Lett. **64**, 2164 (1990).
[18] E. Bychkov and D. L. Price, Sol. State Ionics **136-137**, 1041 (2000).
[19] A. A. Lavrentyev, A. N. Gusatinskii, I. Y. Nikiforov, and N. Y. Safontseva, Physica B **208&209**, 344 (1995).
[20] I. I. Golovach, V. Y. Slivka, V. V. Matyashovskiĭ, N. I. Dovgosheĭ, V. M. Bentsa, and M. I. Golveĭ, Sov. Phys. Solid State **18**, 1930 (1976).
[21] J. Akola, R. O. Jones, S. Kohara, S. Kimura, K. Kobayashi, M. Takata, T. Matsunaga, R. Kojima, and N. Yamada, Phys. Rev. B **80**, 020201(R) (2009).
[22] T. Matsunaga, J. Akola, S. Kohara, T. Honma, K. Kobayashi, E. Ikenaga, R. O. Jones, N. Yamada, M. Takata, and R. Kojima, Nat. Mater. **10**, 129 (2011).
[23] I. Voleská, J. Akola, P. Jóvári, J. Gutwirth, T. Wágner, Th. Vasileiadis, S. N. Yannopoulos, and R. O. Jones, Phys. Rev. B **86**, 094108 (2012).
[24] D. N. Tafen, D. A. Drabold, and M. Mitkova, Phys. Rev. B **72**, 054206 (2005).
[25] B. Prasai and D. A. Drabold, Phys. Rev. B **83**, 094202 (2011).
[26] S.-G. Park, B. Magyari-Köpe, and Y. Nishi, IEEE Electron Device Lett. **32**, 197 (2011).
[27] H. F. Poulsen, H.-B. Neumann, J. R. Schneider, J. Neuefeind, and M. D. Zeidler, J. Non-Cryst. Solids **188**, 63 (1995).
[28] I. A. Blech and B. L. Averbach, Phys. Rev. **137**, A1113 (1965).
[29] H. H. Paalman and J. C. Pings, J. Appl. Phys. **33**, 2635 (1962).
[30] C. N. J. Wagner, in *Liquid Metals, Chemistry and Physics*, edited by S. Z. Beer (Dekker, New York, 1972), p. 57.
[31] K. V. Klementev, J. Phys. D: Appl. Phys. **34**, 209 (2001).
[32] CPMD V3.15 ©IBM Corp 1990-2012, ©MPI für Festkörperforschung Stuttgart 1997-2001, http://www.cpmd.org.
[33] J. P. Perdew, A. Ruzsinszky, G. I. Csonka, O. A. Vydrov, G. E. Scuseria, L. A. Constantin, X. Zhou, and K. Burke, Phys. Rev. Lett. **100**, 136406 (2008).
[34] N. Troullier and J. L. Martins, Phys. Rev. B **43**, 1993 (1991).
[35] G. J. Martyna, M. L. Klein, and M. Tuckerman, J. Chem. Phys. **97**, 2635 (1992).
[36] J. Akola and R. O. Jones, Phys. Rev. B **76**, 235201 (2007).
[37] R. L. McGreevy and L. Pusztai, Mol. Simul. **1**, 359 (1988).
[38] O. Gereben, P. Jóvári, L. Temleitner, and L. Pusztai, J. Optoelectron. Adv. M. **9**, 3021 (2007); Code and executables are available at http://www.szfki.hu/~nphys/rmc++/opening.html
[39] See Supplemental Material at http://link.aps.org/supplemental/10.1103/PhysRevB.89.064202 for figures of (a) pair distribution functions and bond orders in AsS_2 and $AgAsS_2$, (b) partial PDF for cavities in $AgAsS_2$, and (c) a table of cavity coordination numbers.
[40] R. Winter, P. A. Egelstaff, W. C. Pilgrim, and W. S. Howells, J. Phys.: Condens. Matter **2**, SA215 (1990).
[41] R. Winter, W. C. Pilgrim, P. A. Egelstaff, P. Chieux, S. Anlauf, and F. Hensel, Europhys. Lett. **11**, 225 (1990).
[42] R. O. Jones and P. Ballone, J. Chem. Phys. **118**, 9257 (2002). See, in particular, the Supplementary Information.
[43] S. Sen, C. W. Ponader, and B. G. Aitken, J. Non-Cryst. Solids **293-295**, 204 (2001).
[44] S. Soyer-Uzun, C. J. Benmore, J. E. Siewenie, and S. Sen, J. Phys.: Condens. Matter **22**, 115404 (2010).
[45] S. Kohara, J. Akola, H. Morita, K. Suzuya, J. K. R. Weber, M. C. Wilding, and C. J. Benmore, Proc. Natl. Acad. Sci. USA **108**, 14780 (2011).
[46] V. Y. Slivka, Y. M. Vyoschanskiĭ, V. A. Stevanovich, V. S. Gerasimenko, and D. V. Chepur, Sov. Phys. Solid State **24**, 392 (1982).
[47] M. Krbal, T. Wágner, T. Srba, J. Schwarz, J. Orava, T. Kohoutek, V. Zima, L. Beneš, S. O. Kasap, and M. Frumar, J. Non-Cryst. Solids **353**, 1232 (2007).
[48] L. B. Zladkin and Y. M. Markov, Phys. Status Solidi (a) **4**, 391 (1971).
[49] J. M. Besson, J. Cernogora, and R. Zallen, Phys. Rev. B **22**, 3866 (1980).
[50] I. I. Golovach, N. I. Dovgoshei, V. Y. Slivka, L. M. Suslikov, M. I. Golovei, and A. V. Bogdanova, Inorg. Mater. (USSR) **11**, 820 (1975).
[51] A. A. Lavrentiev, B. V. Gabrel'yan, I. Y. Nikiforov, and V. B. Vorzhev, J. Struct. Chem. **46**, 805 (2005).
[52] FEFF8 program, www.feffproject.org.
[53] W. Tang, E. Sanville, and G. Henkelman, J. Phys.: Condens. Matter **21**, 084204 (2009).